The Astrophysical Journal, 700:L88–L91, 2009 August 1 doi:10.1088/0004-637X/700/2/L88

A SELF-CONSISTENT NONLINEAR FORCE-FREE SOLUTION FOR A SOLAR ACTIVE REGION MAGNETIC FIELD

M. S. Wheatland[1] and S. Régnier[2]
[1] Sydney Institute for Astronomy, School of Physics, University of Sydney, NSW 2006, Australia; m.wheatland@physics.usyd.edu.au
[2] School of Mathematics and Statistics, University of St Andrews, St Andrews, Fife KY16 9SS, UK; stephane@mcs.st-andrews.ac.uk
Received 2009 May 8; accepted 2009 June 23; published 2009 July 10

ABSTRACT

Nonlinear force-free solutions for the magnetic field in the solar corona constructed using photospheric vector magnetic field boundary data suffer from a basic problem: the observed boundary data are inconsistent with the nonlinear force-free model. Specifically, there are two possible choices of boundary conditions on vertical current provided by the data, and the two choices lead to different force-free solutions. A novel solution to this problem is described. Bayesian probability is used to modify the boundary values on current density, using field-line connectivity information from the two force-free solutions and taking into account uncertainties, so that the boundary data are more consistent with the two nonlinear force-free solutions. This procedure may be iterated until a set of self-consistent boundary data (the solutions for the two choices of boundary conditions are the same) is achieved. The approach is demonstrated to work in application to *Hinode*/Solar Optical Telescope observations of NOAA active region 10953.

Key words: Sun: corona – Sun: magnetic fields

1. INTRODUCTION

Solar coronal magnetic fields provide the source of energy for solar flares, and there is strong interest in developing methods for accurately modeling these fields, as a basis for improved understanding of solar activity. Spectropolarimetric measurements of magnetically sensitive photospheric lines may be used to infer the vector magnetic field at the photosphere. In principle, these measurements provide boundary values for modeling the overlying solar corona using magnetic field extrapolation techniques. However, in practice basic difficulties prevent the construction of reliable models (Schrijver et al. 2008; DeRosa et al. 2009).

A popular model for the coronal magnetic field in the low-density corona is the force-free model, involving a static balance of magnetic forces (e.g., Sakurai 1981; McClymont et al. 1997). The model is justified by the low ratio of gas pressure to magnetic pressure, or plasma beta, in the solar corona (e.g., Gary 2001). A nonlinear force-free magnetic field $\mathbf{B}$ satisfies $\nabla \times \mathbf{B} = \alpha \mathbf{B}$ and $\mathbf{B} \cdot \nabla \alpha = 0$, where α is the force-free parameter, which is constant along field lines, but varies in space from field line to field line. The boundary conditions for the nonlinear problem consist of a specification of the normal component of $\mathbf{B}$ in the boundary (denoted B_n), together with a specification of α over one polarity (sign) of B_n (e.g., Grad & Rubin 1958; Sakurai 1981; Aly 1989; Amari et al. 2006). The α-boundary condition is equivalent to a specification of the normal component of the electric current density $\mathbf{J} = \alpha \mathbf{B}/\mu_0$ over one polarity of B_n.

Nonlinear force-free boundary value problems are difficult to solve in general. A number of numerical methods have been developed (for a recent review, see Wiegelmann 2008), and demonstrated to work on test cases (e.g., Schrijver et al. 2006; Metcalf et al. 2008). Not all methods uses the boundary conditions on α outlined above. For example, the optimization method (Wheatland et al. 2000; Wiegelmann 2004) and some versions of the magnetofrictional method (e.g., Roumeliotis 1996; Valori et al. 2005) specify all three components of the vector magnetic field in the boundary over both polarities. Although in general this is an over-prescription, if the boundary values are consistent with the force-free model, this does not introduce a problem. A class of methods based on those of Grad & Rubin (1958) uses the boundary conditions on α described above, and the code employed in this paper is a Grad–Rubin, or "current-field iteration" method (for details see Wheatland 2007).

In two recent workshops (Schrijver et al. 2008; DeRosa et al. 2009), a number of nonlinear force-free methods were critically assessed in application to solar vector magnetic field data from the spectropolarimeter (SP) instrument of the Solar Optical Telescope (SOT) on the *Hinode* satellite (Tsuneta et al. 2008). Different methods were found to produce significantly different coronal field solutions for the same active region, and in particular the magnetic energy of the different solutions varied substantially, preventing reliable determination of the magnetic free energy of the active region. The results from individual methods also lacked self-consistency. For example, for the Grad–Rubin methods (Amari et al. 1997, 2006; Wheatland 2007), the two choices of polarity for the boundary conditions on electric current density led to different force-free solutions. Despite this basic problem, nonlinear force-free modeling is often applied to solar boundary data for selected active regions (e.g., Régnier & Priest 2007; Wang et al. 2008; Canou et al. 2009).

Determinations of the photospheric magnetic field transverse to the line of sight are substantially uncertain, and the errors are likely to contribute to the inconsistency problem. However, a more fundamental difficulty is that the magnetic field is unlikely to be force-free at the level of the measurements. The denser photospheric plasma is subject to magnetic, pressure, gravity, and dynamical forces (Metcalf et al. 1995). Necessary conditions for a force-free field may be checked by calculating integrals of the field in the boundary representing the net magnetic flux, and the net force and torque on the field (Molodenskii 1969; Aly 1984, 1989). The integrals are zero for boundary data from a force-free field, but (in general) are found to be nonzero for solar photospheric data. One approach to the problem involves "preprocessing" the data to minimize these integrals (Wiegelmann et al. 2006). However, the conditions

are necessary but not sufficient, and after preprocessing the boundary data are still inconsistent with the force-free equations (DeRosa et al. 2009). Also, preprocessing typically involves smoothing the data, which is undesirable.

An alternative approach to the problem is to calculate a force-free solution (or solutions) with boundary conditions which depart from the observed boundary data, and to then adjust the boundary conditions on the solution(s) until a "best fit" is achieved with the observed boundary data (e.g., Roumeliotis 1996; Aly & Amari 2007). In this Letter we demonstrate such a scheme. The method uses the information on field line connectivity provided by the two force-free solutions constructed from the two choices of boundary conditions on α, and takes into account uncertainties in the α values. Bayesian probability (e.g., Jaynes 2003) is used to adjust the boundary values iteratively until a self-consistent set of values (the two force-free solutions are the same) is achieved.

The layout of the paper is as follows. Section 2 describes the method, and Section 3 presents a simple application to *Hinode*/SOT data for NOAA active region 10953, the subject of a recent nonlinear force-free workshop (DeRosa et al. 2009). Section 4 discusses the results.

2. METHOD

The available solar data are assumed to be a set of values (B_x, B_y, B_z) of the magnetic field over an observed region on the photosphere. We neglect solar curvature, and assume z is the vertical direction, and $z = 0$ is the photospheric plane. Boundary values of the force-free parameter at $z = 0$ may be obtained using $\alpha_0 = \mu_0 J_z / B_z$, where

$$\mu_0 J_z = \frac{\partial B_y}{\partial x} - \frac{\partial B_x}{\partial y} \tag{1}$$

is estimated by finite differences. Uncertainties in the magnetic field components may be used to calculate corresponding uncertainties σ_0 in the estimates of α_0 (e.g., Leka & Skumanich 1999).

As described in Section 1, the values α_0 together with the vertical component B_z of the field provide two sets of boundary values for the force-free problem: one with α_0 chosen on the positive polarity (denoted P), and one with α_0 chosen on the negative polarity (N). The current-field iteration method may be applied using the α_0 values on polarity P, to give one nonlinear force-free solution. Values of the force-free parameter are constant along field lines in a force-free model, so the solution maps values of α_0 at points in P to points in N, at the conjugate foot points of field lines. These mappings define new values α_1 of the force-free parameter over points in N. The current-field iteration procedure may also be applied using the α_0 values on the polarity N as boundary conditions, to give a second nonlinear force-free solution. This solution maps the α_0 values in N to points in P. Hence, it defines new values α_1 of the force-free parameter at points in P. The result of the two solutions is a complete set of values of α_1 (i.e., defined over both P and N). The new values also have associated uncertainties σ_1 obtained by mapping the uncertainty values from the source polarity in each case. Hence, at each point over the observed region we have two possible sets of values: (α_0, σ_0) or (α_1, σ_1).

Bayes's theorem may be used to decide on the most probable single value of the force-free parameter at each boundary point. The theorem may be stated as $\mathcal{P}(M|D, I) \propto \mathcal{P}(D|M, I)\mathcal{P}(M, I)$, where $\mathcal{P}$ denotes a probability, M a model, D data, and I other information. In our context M is the value of α to be decided on, D is the new information from the mappings, i.e., (α_1, σ_1), and I is the information available before the mappings, i.e., (α_0, σ_0). Assuming Gaussian errors we have $\mathcal{P}(D|M, I) \propto \exp[-(\alpha - \alpha_1)^2/(2\sigma_1^2)]$ and $\mathcal{P}(M, I) \propto \exp[-(\alpha - \alpha_0)^2/(2\sigma_0^2)]$. Writing $\mathcal{L}(\alpha) = -\ln \mathcal{P}(M|D, I)$, we have

$$\mathcal{L}(\alpha) = \frac{(\alpha - \alpha_0)^2}{2\sigma_0^2} + \frac{(\alpha - \alpha_1)^2}{2\sigma_1^2}, \tag{2}$$

ignoring an additive constant. The most probable value of α, which we denote by α_2, is then given by $\mathcal{L}'(\alpha_2) = 0$:

$$\alpha_2 = \frac{\alpha_0/\sigma_0^2 + \alpha_1/\sigma_1^2}{1/\sigma_0^2 + 1/\sigma_1^2}, \tag{3}$$

i.e., an uncertainty-weighted average value. A corresponding uncertainty σ_2 may be defined assuming Gaussian behavior in the vicinity of the peak by $\sigma_2 = [\mathcal{L}''(\alpha_2)]^{-1/2}$, yielding

$$\sigma_2 = \left(\frac{1}{\sigma_0^2} + \frac{1}{\sigma_1^2}\right)^{-1/2}. \tag{4}$$

If the uncertainties in α_0 (and hence also α_1) are assumed to be equal at all points, then $\alpha_2 = \frac{1}{2}(\alpha_0 + \alpha_1)$, the simple average.

The resulting values of α_2 will still be inconsistent with a force-free field, in general, but they are expected to be closer to consistency. The process may then be repeated, using the α_2 values in the place of α_0. Two solutions are calculated, one from each polarity, and then the field line mappings of the solutions and the values (α_2, σ_2) define a new set of values (α_3, σ_3). Equations (3) and (4) are applied again, leading to a new set of values (α_4, σ_4). This process is iterated. The construction of a pair of solutions, and their use to obtain a new α-map, represents a "self-consistency cycle." For convenience we label the two force-free solutions constructed during each cycle by an index k, so that the first cycle involves solution numbers $k = 1$ and $k = 2$. It is expected that the procedure will converge after a number of self-consistency cycles, in the sense that the two solutions from the different polarities become identical. The result is expected to be a single force-free solution, with a minimum departure from the observations.

3. APPLICATION TO *HINODE*/SOT DATA

To demonstrate the method, we consider *Hinode*/SOT data from the recent force-free workshop, for NOAA active region 10953, observed at 22:30 UT on 2007 April 30. The data are described in DeRosa et al. (2009), and consist of field components (B_x, B_y, B_z) on a 320×320 grid spanning a 185.6 Mm^2 area. The *Hinode* data fill only part of the 320×320 field of view, with the additional B_z values derived from a line-of-sight magnetogram from the Michelson Doppler Interferometer (MDI) instrument on the *Solar and Heliospheric Observatory* (*SOHO*) spacecraft (Scherrer et al. 1995). The data used here are not preprocessed, and no smoothing is applied. Values of α_0 are obtained by centered differencing of B_x and B_y values according to Equation (1), for all points with $|B_z| > 0.01 \times \max(B_z)$. Values of α_0 are zero for points in the field of view corresponding to the MDI data. Uncertainties are not available for the photospheric field measurements, so we assume that the uncertainties in the α_0 values are equal at all points.

The current-field iteration method (Wheatland 2007) is used to calculate force-free solutions from the boundary values for

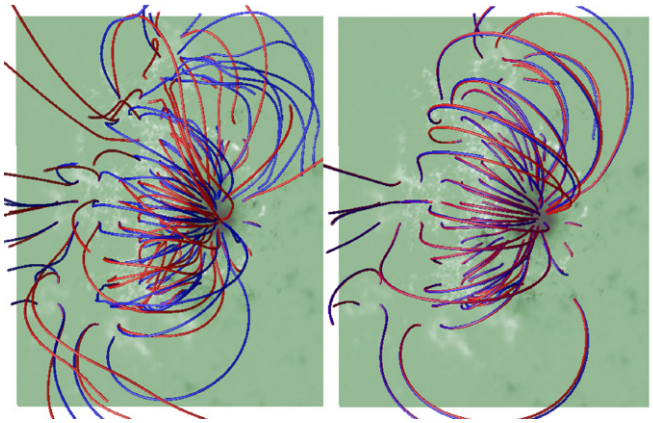

Figure 1. Left panel: overlay of field lines for the two force-free solutions constructed using boundary conditions on current density taken from the positive polarity (blue lines) and from the negative polarity (red lines), using the original boundary data (solutions $k = 1$ and $k = 2$). Right panel: overlay of the field lines for the two solutions after 10 self-consistency cycles (solutions $k = 19$ and $k = 20$). The image in the background of each panel shows the boundary values of B_z, with positive polarity areas appearing light, and negative polarity areas dark.

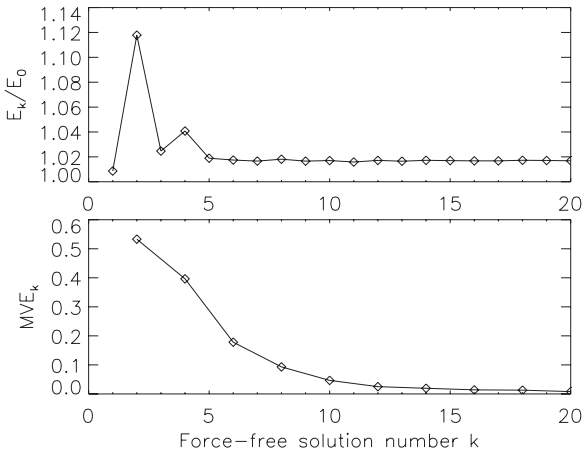

Figure 2. Upper panel: the magnetic energy E_k of each force-free solution, in units of the energy of the potential field E_0, over the 10 self-consistency cycles. Solutions $k = 1, 3, \ldots, 19$ are constructed using α values on the positive polarity, and solutions $k = 2, 4, \ldots, 20$ using values on the negative polarity. Lower panel: the mean vector error, quantifying the discrepancy between the two fields constructed at each cycle.

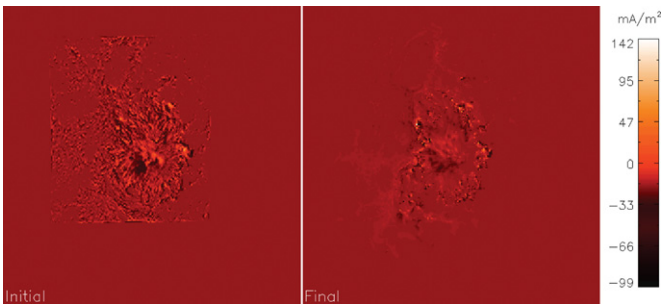

Figure 3. Boundary conditions on electric current density in the observations (left panel) and in the solution after 10 self-consistency cycles (right panel).

α on the two polarities, for 10 self-consistency cycles. Each solution involves 20 Grad–Rubin iterations, sufficient to achieve approximate convergence. The solutions are constructed on a $320 \times 320 \times 256$ grid. During the construction of each solution, points on the grid threaded by field lines which cross the sides or top boundaries of the computational volume (including points on the grid in the lower boundary) have α set to zero. This provides a simple solution to the problem of "missing information" associated with the absence of boundary conditions on the sides and top of the computational volume. After each cycle, a new α-map is constructed according to Equation (3), with the assumption of constant uncertainties.

The procedure is found to converge: the fields constructed from the two choices of boundary conditions are very similar after 10 cycles. Figure 1 illustrates field lines for the two solutions at the first and the last cycles. The left panel shows the two force-free fields at the first cycle, constructed from the original boundary data. The blue solution ($k = 1$) uses α_0 values on the positive polarity and the red solution ($k = 2$) uses α_0 values on the negative polarity (this is similar to the "Wh$^-$" solution from DeRosa et al. (2009), except that the Wh$^-$ solution used preprocessed boundary data). The blue and red field lines are quite different. The red field lines are more distorted, suggesting that this solution is more non-potential. The right panel shows the corresponding solutions at the tenth cycle (solutions $k = 19$ and $k = 20$). The two solutions are very similar. The image in the background of each panel shows the boundary values of B_z, with positive polarity areas appearing light, and negative polarity dark.

Figure 2 illustrates two quantitative measures of the difference between the two solutions at each cycle. The upper panel shows the magnetic energy E_k of each solution, in units of the energy E_0 of the potential field. The field constructed from the values of α_0 on the negative polarity ($k = 2$) has substantially more energy than the field constructed using the positive polarity ($k = 1$), as suggested by the appearance of the field lines in Figure 1. After 10 self-consistency cycles the energies of the two solutions are very similar (they differ by $< 0.03\%$). The dimensional energy of the potential field is $E_0 = 8.96 \times 10^{25}$ J, and the energy of the final fields obtained by the self-consistency procedure is $E_f = 9.11 \times 10^{25}$ J. Hence, the free energy of the magnetic field for the final solutions is $E = 1.5 \times 10^{24}$ J. The lower panel in Figure 2 shows the mean vector error between solutions k and $k - 1$, defined by (Schrijver et al. 2006)

$$MVE_k = \frac{1}{N_x N_y N_z} \sum_i \frac{|\mathbf{B}_i^{(k)} - \mathbf{B}_i^{(k-1)}|}{|\mathbf{B}_i^{(k-1)}|}, \qquad (5)$$

where i runs over the points on the computational grid. The mean vector error is reduced by more than a factor of 60 by the procedure.

It is also interesting to examine the changes in the boundary conditions on current, and in the boundary components B_x and B_y. Figure 3 shows the vertical electric current density $J_z = \alpha B_z/\mu_0$ at the first and last cycles. The left panel shows the observed values of J_z and the right panel shows the values after the last cycle. The currents have been reduced in magnitude overall by the averaging in the self-consistency procedure, but it is notable that basic structures present in the original data remain. The changes in the horizontal field are substantial: the rms change in B_x across the entire field of view is 120 G and the rms change in B_y is 100 G. This is to be expected given the gross discrepancy between the two initial solutions (left panel in Figure 1). Some part of the change is due to the artificial construction of the boundary data, specifically the embedding of the *Hinode*/SOT data within a set of *SOHO*/MDI data with a larger field of view. Boundary points corresponding to the MDI data have $\alpha_0 = 0$, but during the self-consistency procedure

nonzero values of α may be mapped to these points, leading to significant changes in B_x and B_y. For comparison, we note that the preprocessing procedure used at the recent nonlinear force-free workshop (DeRosa et al. 2009) introduced rms changes in B_x and B_y of about 60 G, as well as an rms change in B_z of about 80 G (values of B_z are unchanged in the self-consistency procedure).

4. DISCUSSION

A method for calculating a self-consistent nonlinear force-free solution from solar photospheric vector magnetic field boundary data is described. The "self-consistency" procedure resolves the fundamental problem that the solar data define two different force-free solutions. The method involves constructing the two solutions and then adjusting the boundary conditions on the force-free parameter using the field line connectivity defined by the solutions, taking into account observational uncertainties. Iteration of the procedure leads to a set of boundary data for which there is only one force-free solution. The method is demonstrated to work in application to *Hinode*/SOT data for NOAA active region 10953.

The results for active region 10953 should be regarded as providing a proof of concept, rather than as the construction of a completely realistic model, due to a number of limitations. For example, the results could be improved by assigning uncertainties to the α values, so that more reliable boundary conditions on the electric current density are treated preferentially. It is difficult to assign uncertainty estimates which are correct in an absolute sense. An advantage of the present method is that, according to Equation (3), only the relative sizes of the uncertainties need to be correct. Another limitation of the present calculation is the embedding of *Hinode*/SOT data in a larger (*SOHO*/MDI) field of view for which the boundary values of α are zero. For field lines with one foot point in the MDI region, the averaging in the self-consistency procedure reduces $|\alpha|$ by comparison with the value at the *Hinode*/SOT foot point. It is likely that these limitations account in part for the relatively small free energy of the final field.

The self-consistency procedure provides a way to use the observed boundary information on electric currents from both polarities, which is preferable to discarding the information from one polarity. It should be noted that the magnetofrictional method (e.g., Valori et al. 2005) and the optimization method (e.g., Wiegelmann 2004) already use the boundary data on currents from both polarities. However, the difference between the magnetofrictional/optimization approaches and the present method is that the present method determines a force-free solution and a set of boundary conditions that are consistent with the force-free model. If the observed boundary data are inconsistent with the force-free model the magnetofrictional/optimization methods will not achieve this, without additional modification (see Aly & Amari (2007) for a suggested approach, in the context of the optimization method).

In future work the self-consistency procedure will be investigated in more detail, via application to test cases with inconsistent boundary data. This should permit characterization of the convergence of the scheme. Other solar (and solar-like) data will also be examined, including the other cases from the nonlinear force-free workshops (Metcalf et al. 2008; Schrijver et al. 2008), and the method will be applied with uncertainties when available.

The self-consistency procedure is applicable to a wealth of archival data from ground-based observatories, including the National Solar Observatory's Synoptic Optical Long-term Solar Investigations of the Sun Vector Spectromagnetograph (SOLIS/VSM), as well as satellite data from *Hinode*/SOT and the Helioseismic and Magnetic Imager (HMI) on NASA's *Solar Dynamics Observatory* (SDO), due to be launched in 2009. Reliable coronal magnetic field models should greatly enhance the science value of data obtained from these facilities, permitting investigation of diverse aspects of the physics of the solar atmosphere and of solar activity.

Stephane Régnier acknowledges the support of a Royal Society Short Visit Grant during a visit to the University of Sydney.

Facilities: Hinode, *SOHO*.

REFERENCES

Aly, J. J. 1984, ApJ, 283, 349
Aly, J. J. 1989, Sol. Phys., 120, 19
Aly, J. J., & Amari, T. 2007, Geophys. Astrophys. Fluid Dyn., 101, 249
Amari, T., Aly, J. J., Luciani, J. F., Boulmezaoud, T. Z., & Mikic, Z. 1997, Sol. Phys., 174, 129
Amari, T., Boulmezaoud, T. Z., & Aly, J. J. 2006, A&A, 446, 691
Canou, A., Amari, T., Bommier, V., Schmieder, B., Aulanier, G., & Li, H. 2009, ApJ, 693, L27
DeRosa, M. L., et al. 2009, ApJ, 696, 1780
Gary, G. A. 2001, Sol. Phys., 203, 71
Grad, H., & Rubin, H. 1958, in Proc. 2nd Int. Conf. on Peaceful Uses of Atomic Energy, Vol. 31, (Geneva: UN) 190
Jaynes, E. T. 2003, in in Probability Theory, ed. G. L. Bretthorst, (Cambridge: Cambridge Univ. Press)
Leka, K. D., & Skumanich, A. 1999, Sol. Phys., 188, 3
McClymont, A. N., Jiao, L., & Mikic, Z. 1997, Sol. Phys., 174, 191
Metcalf, T. R., Jiao, L., McClymont, A. N., Canfield, R. C., & Uitenbroek, H. 1995, ApJ, 439, 474
Metcalf, T. R., et al. 2008, Sol. Phys., 247, 269
Molodenskii, M. M. 1969, Sov. Astron., 12, 585
Régnier, S., & Priest, E.R. 2007, ApJ, 669, L53
Roumeliotis, G. 1996, ApJ, 473, 1095
Sakurai, T. 1981, Sol. Phys., 69, 343
Scherrer, P. H., et al. 1995, Sol. Phys., 162, 129
Schrijver, C. J., et al. 2006, Sol. Phys., 235, 161
Schrijver, C. J., et al. 2008, ApJ, 675, 1637
Tsuneta, S., et al. 2008, Sol. Phys., 249, 167
Valori, G., Kliem, B., & Keppens, R. 2005, A&A, 433, 335
Wang, H., Jing, J., Tan, C., Wiegelmann, T., & Kubo, M. 2008, ApJ, 687, 658
Wheatland, M. S. 2007, Sol. Phys., 245, 251
Wheatland, M. S., Sturrock, P. A., & Roumeliotis, G. 2000, ApJ, 540, 1150
Wiegelmann, T. 2004, Sol. Phys., 219, 87
Wiegelmann, T. 2008, J. Geophys. Res. (Space Physics), 113, 3
Wiegelmann, T., Inhester, B., & Sakurai, T. 2006, Sol. Phys., 233, 215